

Reassessment of transient permeability measurement for tight rocks: The role of boundary and initial conditions

Yue Wang^a, Zhiguo Tian^a, Steffen Nolte^b, Alexandra Amann-Hildenbrand^b,
Bernhard M. Krooss^b, Moran Wang^{a,*}

^a Department of Engineering Mechanics and CNMM, Tsinghua University, Beijing, 100084, China

^b Institute of Geology and Geochemistry of Petroleum and Coal, Energy and Mineral Resources Group (EMR), RWTH Aachen University, Lochnerstr. 4-20, Aachen, D-52056, Germany

ARTICLE INFO

Keywords:

Pulse-decay method
Gas permeability
Boundary condition
Initial condition
Separation of variables

ABSTRACT

The pulse-decay method is one of the most widely used transient methods for permeability measurements. Though many modified pulse-decay methods with various experimental designs have been proposed, the theoretical analysis is still insufficient, especially from the perspective of the boundary and initial conditions. In terms of boundary conditions, the tests can be conducted with a reservoir of finite volume on one side of the sample and a reservoir of “zero”, finite, or “infinite” volume on the other side. Common initial conditions differ in terms of the pore pressure within the sample at the start of the test, which can be either equal to the downstream or the upstream reservoir pressure. For the first time, the method of separation of variables is used to obtain the analytical solutions of the pulse-decay methods and assess the specific effects of boundary and initial conditions. The results indicate that if the pressure difference between two ends of the sample is less than 10 %, the slope of the semi-logarithmic plot of pressure versus time is solely determined by the boundary conditions (pore volume/reservoir volume ratios), and the intercept depends on both the boundary and initial conditions. We show that the requirement that a new pressure pulse cannot be applied before the previous pulse subsides is unnecessary and the restriction on the pulse size can be relaxed to some extent. The duration of the pulse-decay tests is mainly determined by the boundary conditions, and the influence of initial conditions decreases as the reservoir volumes increase. The error in the permeability evaluation caused by the inaccuracy of pore and reservoir volume measurements is also discussed.

1. Introduction

Permeability denotes the ability of rocks to transmit fluids upon the action of a pressure gradient. The precise, reliable, and rapid determination of permeability coefficients of low-permeable rocks is of increasing importance in geotechnical applications, such as radioactive waste disposal (Birkholzer et al., 2012; Miller et al., 2000; Yang and Wang, 2019), carbon dioxide storage (Busch et al., 2008; House et al., 2006; Song and Zhang, 2013), and unconventional oil/gas exploitation (Cui et al., 2009; Liu and Zhang, 2019; Lv et al., 2017; Pan et al., 2010; Wang et al., 2018). In the laboratory, permeability measurements are conducted either by steady-state or transient methods (Hannon, 2016; Sander et al., 2017; Wang et al., 2019). In the steady-state method, the flow rate through the sample under a constant pressure gradient is measured. Although the steady-state method works successfully for

high-permeable rocks, it is inadequate for low-permeable (“tight”) rocks, because the flow rate is usually too small to be recorded precisely, and the establishment of the steady state is time-consuming. Therefore, the transient method, where the pressure variation rather than the flow rate is used for permeability evaluation, is the preferred option for permeability measurements on tight rocks (Gaus et al., 2019; Heller et al., 2014; Pan and Connell, 2012).

The pulse-decay method, proposed by Brace et al. (1968), has become one of the most widely used transient methods for permeability measurements (Sander et al., 2017). In the original pulse-decay test, a sample is connected to two gas reservoirs at its two ends and the entire system is in pressure equilibrium before the test. The pressure in one reservoir is then changed instantaneously to create an initial pressure difference, and the resulting pressure variations in both reservoirs are recorded (see Fig. 1). The permeability coefficient is determined by

* Corresponding author.

E-mail address: mrwang@tsinghua.edu.cn (M. Wang).

<https://doi.org/10.1016/j.jngse.2021.104173>

Received 18 March 2021; Received in revised form 19 July 2021; Accepted 24 July 2021

Available online 28 July 2021

1875-5100/© 2021 Elsevier B.V. All rights reserved.

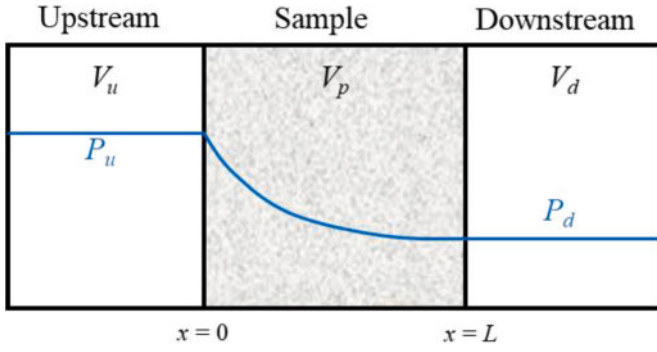


Fig. 1. Scheme of the pulse-decay test with upstream (high initial pressure $P_u(0)$) and downstream (low initial pressure $P_d(0)$) compartments adjacent to the sample. The sample is L long with a pore volume of V_p . The upstream and downstream reservoir volumes are V_u and V_d , respectively.

fitting the analytical solution to the measured pressure transients (Pan and Connell, 2012). The analytical solution obtained by Brace et al. (1968) is valid when the pore volume of the sample is much smaller than the gas reservoir volumes. Hsieh et al. (1981) and Dicker and Smits (1988) extended Brace et al.'s solution and obtained a general solution through Laplace transformation. Some modified pulse-decay methods with various experimental designs have also been developed. Yang et al. (2015) proposed a method where one end of the sample is connected to the gas reservoir, while the other end is sealed. Metwally and Sondergeld (2011) and Heller et al. (2014) evaluated the permeability by recording the downstream pressure changes after increasing the upstream pressure instantaneously and keeping it constant. All the pulse-decay methods mentioned above share the same governing equation, and the differences lie in boundary and initial conditions. Although these methods have been used in practice, a detailed theoretical analysis, especially the investigation of the specific effects of the boundary and initial conditions, is still insufficient.

In this study, we discuss in detail the three boundary conditions and the two initial conditions widely used in pulse-decay methods. The method of separation of variables is used to obtain the analytical solution and theoretically investigate the effects of boundary and initial conditions. The essentiality of uniform initial pressure within the sample and small initial pressure difference is also discussed. The theoretical results are verified by numerical simulation and experimental data. The influence of boundary and initial conditions on the time expenditure and accuracy for pulse-decay tests are discussed in detail.

2. Theoretical analysis

a) Classification of boundary and initial conditions

The flow rate under a pressure gradient is described by Darcy's Law:

$$v = -\frac{k_{app}}{\mu} \frac{\partial P}{\partial x} \quad (1)$$

where v [$\text{m}\cdot\text{s}^{-1}$] is the flow rate, k_{app} [m^2] the apparent permeability of the sample, μ [$\text{Pa}\cdot\text{s}$] the dynamic viscosity of the testing gas, and $P(x, t)$ [Pa] is the gas pressure (also referred to as the pore pressure) at position x [m] and time t [s].

According to the law of the conservation of mass, for every differential volume in the sample, the mass increase of gas stored in the pore space should be equal to the difference between the inlet and outlet mass flux:

$$\frac{\partial}{\partial t}(\rho\varphi) + \frac{\partial}{\partial x}(\rho v) = 0 \quad (2)$$

where ρ [$\text{kg}\cdot\text{m}^{-3}$] is the gas density and φ is the porosity of the sample.

Combining Eqs. (1) and (2), we have:

$$\frac{\partial}{\partial t}(\rho\varphi) = \frac{\partial}{\partial x} \left(\rho \frac{k_{app}}{\mu} \frac{\partial P}{\partial x} \right) \quad (3)$$

Eq. (3) is nonlinear because the variables in it are generally pressure-dependent. For instance, the apparent permeability of the sample change with gas pressure due to the poro-elastic and slippage effects (Chen et al., 2019; Dong et al., 2010; Zoback and Byerlee, 1975). Since the upstream and downstream pressures are different during the pulse-decay measurement, these pressure-dependent variables vary along the length of the sample. However, as pointed out by Brace et al. (1968) that if the relative pressure difference between two ends of the sample is very small, the variations of the pressure-dependent variables induced by non-uniform pressure may be neglected and then Eq. (3) can be simplified to a linear form:

$$\frac{\partial P}{\partial t} = \frac{k_{app}}{\beta\mu\varphi} \frac{\partial^2 P}{\partial x^2} \quad (4)$$

where $\beta = \partial \ln \rho / \partial P$ [Pa^{-1}] is the gas compressibility. By performing pulse-decay measurements on one core sample under a variety of pressure differences, Walder and Nur (1986) proved that the linear governing equation applies when the relative pressure difference across the sample is less than 10 %, which is now accepted by many researchers as the experimental guideline to choose the pressure difference used in pulse-decay tests (Akkutlu and Fathi, 2012; Bhandari et al., 2015; Biliotte et al., 2008; Cui et al., 2009; Heller et al., 2014).

The linearity brings convenience to theoretical analysis. Eq. (4) has been adopted by most studies, including the current one, as the starting point to investigate the pulse-decay method. All the pressure-dependent variables (k_{app} , φ , β , μ) in Eq. (4) are regarded as constants, and their values are taken under the mean pore pressure P_{mean} . Moreover, k_{app} and φ also depend on the confining pressure P_c applied to the sample. In summary, we have:

$$k_{app} = k_{app}(P_{mean}, P_c), \varphi = \varphi(P_{mean}, P_c), \beta = \beta(P_{mean}), \mu = \mu(P_{mean}) \quad (5)$$

and the detailed expression for $k_{app}(P_{mean}, P_c)$ can be determined by performing pulse-decay measurements under different P_{mean} and P_c (Fink et al., 2017; Hu et al., 2020; Pang et al., 2017).

In order to obtain the analytical solution of Eq. (4), the boundary conditions and the initial pressure distribution within the sample must be defined. The three potential single-sided boundary conditions on the upstream and downstream sides can be summarized as follows (Sander et al., 2017):

Upstream:	Downstream:
(i) $\frac{\partial P}{\partial t} \Big _{x=0} = \frac{k_{app}}{\beta\mu\varphi L} \frac{V_p}{V_u} \frac{\partial P}{\partial x} \Big _{x=0}$	(i) $\frac{\partial P}{\partial t} \Big _{x=L} = \frac{k_{app}}{\beta\mu\varphi L} \frac{V_p}{V_d} \frac{\partial P}{\partial x} \Big _{x=L}$
(ii) $\frac{\partial P}{\partial x} \Big _{x=0} = 0$	(ii) $\frac{\partial P}{\partial x} \Big _{x=L} = 0$
(iii) $\frac{\partial P}{\partial t} \Big _{x=0} = 0$	(iii) $\frac{\partial P}{\partial t} \Big _{x=L} = 0$

(6)

Here L [m] is the length of the cylindrical sample, A [m^2] the sample's cross-sectional area, $V_p = LA\varphi$ [m^3] the sample's pore volume, V_p and V_d [m^3] the volumes of the upstream and downstream reservoir, respectively, and $P_u(0)$ and $P_d(0)$ [Pa] are the initial upstream and downstream pressures, respectively.

The single-sided boundary conditions (i) in Eq. (6) are derived by combining the mass conservation equation and Darcy's law for reservoirs of finite volume on the upstream or downstream side. The single-sided boundary condition (ii) applies when one end of the sample is sealed, and (iii) applies when the pressure in one reservoir is kept constant. Mathematically, the single-sided boundary condition (ii) and (iii) can be regarded as the limiting cases of (i) where the reservoir volume is

zero or infinite, respectively. Therefore, the boundary conditions used in the pulse-decay test can be marked with the reservoir volumes (see Table 1).

In theory, nine possible combinations can be constructed because there are three single-sided boundary conditions for both upstream and downstream. However, only five of these can be realized experimentally and can be divided into three categories (see Table 1).

The two-element array enclosed in parenthesis in Table 1 denotes the boundary conditions of the pulse-decay method, where the first element represents the single-sided boundary condition on the upstream side and the second element refers to the downstream one. Here, $a = V_p/V_u$ is the ratio of sample pore volume to the upstream reservoir volume, and $b = V_p/V_d$ is the ratio of pore volume to the downstream reservoir volume. Zero or infinite values indicate that the corresponding end of the sample is sealed ("zero" reservoir volume) or kept at constant pressure ("infinite" reservoir volume), respectively. Otherwise, the corresponding end is connected to a reservoir of finite volume.

The initial conditions here refer to the pressure distribution within the system immediately after the application of a pressure pulse. To evaluate the permeability of the sample under different stress conditions, a series of pressure pulses need to be applied. The prestressing and other sample preparation works are considered to be completed prior to the tests (Sander et al., 2017). Before applying a new pressure pulse, it is required in many studies that the previous one has been eliminated and the pressure within the sample is uniform (Heller et al., 2014). Therefore, we have two initial conditions in pulse-decay methods,

$$\text{Empty:} \quad \text{Loaded:} \\ \text{(I) } P(x,0) = \begin{cases} P_u(0), & x=0 \\ P_d(0), & 0 < x \leq L \end{cases} \quad \text{(II) } P(x,0) = \begin{cases} P_u(0), & 0 \leq x < L \\ P_d(0), & x=L \end{cases} \quad (7)$$

The initial condition (I) is realized by increasing upstream pressure and the initial condition (II) is realized by decreasing the upstream pressure. In other words, the initial condition (I) represents applying a "positive" pressure pulse to the upstream reservoir and the initial condition (II) represents applying a "negative" one to the downstream. Based on the initial amount of gas stored in the sample (see Fig. 2), in the following discussions, the initial condition (I) and (II) are also denoted as "Empty" and "Loaded", respectively. Here we are interested in the relative distribution rather than the absolute value of the pressure within the system. Therefore, when comparing different initial conditions, the initial upstream and downstream pressure is kept equal respectively, and the relative pressure difference is assumed to be less than 10%. The case with a relative pressure difference of more than 10% is discussed in section 3.2.

By combining the different boundary and initial conditions, eight types of pulse-decay procedures can be realized experimentally (see Table A-1 in the Appendix). In previous studies (Dicker and Smits, 1988; Hsieh et al., 1981), Laplace transformation was used to solve the equations and obtain the analytical solutions. However, in Laplace transformation, the initial conditions are substituted into the boundary conditions, so the specific effects of the boundary and initial conditions cannot be separated. In this study, we chose the method of separation of variables to investigate the specific effects of the boundary and the initial conditions on the analytical solutions.

b) The method of separation of variables

Table 1
Three categories of boundary conditions.

Category	Description	Boundary conditions
1	Two reservoirs of finite volume	(a, b)
2	One side of the sample kept at constant pressure	(a, ∞), (∞, b)
3	One side of the sample sealed	(a, 0), (b, 0)

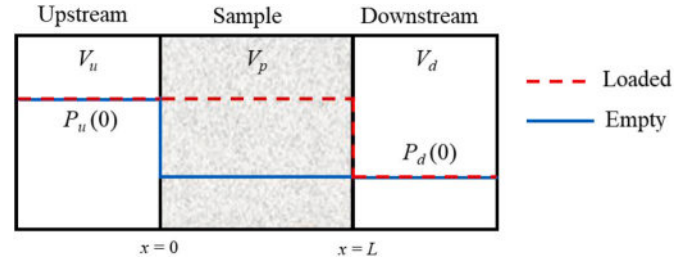


Fig. 2. Scheme of the two initial conditions used in pulse-decay test. The initial pressure within the sample is either equal to the initial upstream pressure $P_u(0)$, or the initial downstream pressure $P_d(0)$. These two initial conditions are denoted as "Loaded" and "Empty", respectively.

The method of separation of variables is a powerful tool in solving partial differential equations (Riley et al., 2002). The essential feature of this method is to replace the partial differential equation with a set of ordinary differential equations, which are then solved subject to the boundary and initial conditions.

For ease of derivation, the following dimensionless variables with subscript D are defined,

$$x_D = \frac{x}{L}, \quad t_D = \frac{k_{app}t}{\beta\mu\phi L^2}, \quad P_D = \frac{P - P_d(0)}{P_u(0) - P_d(0)}, \quad a = \frac{LA\phi}{V_u}, \quad b = \frac{LA\phi}{V_d} \quad (8)$$

where x_D , t_D , P_D represent the dimensionless counterpart of x , t , P , respectively, and a , b represent the ratios of pore volume to upstream and downstream reservoir volume, respectively. With these dimensionless variables, the dimensionless form of the governing equation (4) is obtained,

$$\frac{\partial P_D}{\partial t_D} = \frac{\partial^2 P_D}{\partial x_D^2} \quad (9)$$

The method of separation of variables assumes that the unknown P_D , which depends on x_D and t_D , has a product form,

$$P_D(x_D, t_D) = X(x_D)T(t_D) \quad (10)$$

Substituting this product into Eq. (9), and the partial differential equation separates into two ordinary differential equations,

$$\frac{T'}{T} = \frac{X''}{X} = -\theta_m^2 \quad (11)$$

where $-\theta_m^2$ is called the separation constant. The solutions of the ordinary differential equations in Eq. (11) are

$$T = e^{-\theta_m^2 t_D}, \quad X = A \sin(\theta_m x_D) + B \cos(\theta_m x_D) \quad (12)$$

where A and B are arbitrary constant. It is noted that the negative sign in the separation constant helps to prevent T from growing to infinity over time.

Then Eq. (10) is substituted into the boundary conditions. Without loss of generality, the boundary conditions of finite volume reservoirs (Category 1 in Table 1) are considered here,

$$\left. \frac{\partial P_D}{\partial t_D} \right|_{x_D=0} = a \left. \frac{\partial P_D}{\partial x_D} \right|_{x_D=0} \Leftrightarrow X(0)T' = aX'(0)T \quad (13)$$

$$\left. \frac{\partial P_D}{\partial t_D} \right|_{x_D=1} = -b \left. \frac{\partial P_D}{\partial x_D} \right|_{x_D=1} \Leftrightarrow X(1)T' = -bX'(1)T \quad (14)$$

Combining Eqs. (12)–(14), we have,

$$-\theta_m B = aA \quad (15)$$

$$\tan \theta_m = \frac{(a+b)\theta_m}{\theta_m^2 - ab} \quad (16)$$

Eq. (16) has an infinite number of roots and θ_m is denoted as the m^{th} non-negative one. It is easy to check that $\theta_0 = 0$. Noting that θ_m ($m \geq 1$) are solely determined by the volume ratios between pore and reservoirs (a and b) that appear in the boundary conditions, since the initial condition has not been used yet.

By leaving out the arbitrary multiplicative constant, a series of solutions (called eigenfunctions) with the product form and satisfying the governing equation and boundary conditions are obtained,

$$P_0 = 1, P_m = [\theta_m \sin(\theta_m x_D) + a \cos(\theta_m x_D)]e^{-\theta_m^2 t_D} \quad (m \geq 1) \quad (17)$$

To find the solution satisfying the initial condition, all the eigenfunctions in Eq. (17) are superposed linearly,

$$P_D(x_D, t_D) = A_0 + \sum_{m=1}^{\infty} A_m [\theta_m \sin(\theta_m x_D) + a \cos(\theta_m x_D)]e^{-\theta_m^2 t_D} \quad (18)$$

where A_m ($m \geq 0$) are constants to be determined. By letting $t_D = 0$, Eq. (18) becomes,

$$P_D(x_D, 0) = A_0 + \sum_{m=1}^{\infty} A_m [\theta_m \sin(\theta_m x_D) + a \cos(\theta_m x_D)] \quad (19)$$

The left-hand side of Eq. (19) is the initial condition, and the right-hand side is the orthogonal expansion of the initial condition in terms of the eigenfunctions. The orthogonality between two eigenfunctions is defined as

$$ab \int_0^1 P_n(x_D, 0)P_m(x_D, 0)dx_D + aP_n(1, 0)P_m(1, 0) + bP_n(0, 0)P_m(0, 0) = 0 \quad (n \neq m) \quad (20)$$

Then the constants A_m ($m \geq 0$) can be calculated through the initial condition as:

$$A_m = \frac{ab \int_0^1 P_D(x_D, 0)P_m(x_D, 0)dx_D + aP_D(1, 0)P_m(1, 0) + bP_D(0, 0)P_m(0, 0)}{ab \int_0^1 [P_m(x_D, 0)]^2 dx_D + a[P_m(1, 0)]^2 + b[P_m(0, 0)]^2}, \quad (m \geq 0) \quad (21)$$

Substituting the detailed form of initial condition $P_D(x_D, 0)$ into Eq. (21), the expressions of A_m ($m \geq 0$) and therefore that of $P_D(x_D, t_D)$ in Eq. (18) can be obtained. It is easy to check that A_0 is the dimensionless equilibrium pressure. The analytical solutions of various pulse-decay methods with different boundary and initial conditions are listed in Table A-1 of the appendix.

Combining Eqs. (16) and (21), we can conclude the effects of the boundary and initial conditions on the analytical solutions of the pulse-decay methods:

- (1) The boundary conditions solely determine θ_m ($m \geq 1$) and affect A_m ($m \geq 0$).
- (2) The initial condition only affects A_m ($m \geq 0$).

In practice, the pressure difference, rather than the single upstream or downstream pressure, is usually used for permeability evaluation,

$$\Delta P_D(t) = P_D(0, t) - P_D(1, t) = \sum_{m=1}^{\infty} A_m (a - \theta_m \sin \theta_m - a \cos \theta_m) e^{-\frac{\theta_m^2 k}{\beta \mu \phi L^2} t} \quad (22)$$

Though the solution (22) is valid at any time, it is not easy to be used directly due to its complex form of an infinite series. Noting when time t is large, the high order terms with $m \geq 2$ become negligible and only the

first term remains. Therefore, Eq. (22) can be simplified at the late-time stage of the test,

$$\Delta P_D(t) \approx A_1 (a - \theta_1 \sin \theta_1 - a \cos \theta_1) e^{-\frac{\theta_1^2 k}{\beta \mu \phi L^2} t} \quad (23)$$

which is referred to as the late-time solution in the literature (Jones and Owens, 1980; Jones, 1997).

Shown in Fig. 3(a) are graphs of the dimensionless pressure transients in the upstream and downstream compartments for a pulse-decay test where $a = b = 1$. The graphs of the full general solution Eq. (22) and the late-time solution Eq. (23) in terms of the differences of the dimensionless pressures are superimposed in Fig. 3(b) and (c) (semi-logarithmic plot). It is found that the late-time solution is a good approximation of the full general solution shortly after the start of the test. Only a small deviation is observed in the semi-logarithmic plot for $t_D < 0.05$.

Taking logarithm of Eq. (23), we have

$$\ln \Delta P_D(t) \approx f + \alpha t \quad (24)$$

where

$$f = \ln[A_1 (a - \theta_1 \sin \theta_1 - a \cos \theta_1)] \quad (25)$$

$$\alpha = -\frac{\theta_1^2 k_{app}}{\beta \mu \phi L^2} \quad (26)$$

Eq. (24) indicates that in the late-time stage, the logarithm of the pressure difference decreases linearly along time with the slope α and the intercept f (see Fig. 3(c)). The expressions for f and α are given in Eqs. (25) and (26), respectively.

By transforming Eq. (25), we find that the slope α can be used to evaluate the permeability coefficient, while the intercept f plays no role:

$$k_{app}(P_{mean}, P_c) = -\frac{\alpha \beta \mu \phi L^2}{\theta_1^2} \quad (27)$$

Comparing Eqs. (25) and (26), we note that except for the physical properties of the sample (k_{app} , ϕ , L) and test fluids (β , μ), the slope α only depends on θ_1 , which is determined by the pore volume/reservoir volume ratios (a and b) that appearing in the boundary conditions (see Eq. (16)). However, the intercept f is a function of A_1 and θ_1 , and thus depends on both the boundary and initial conditions. Therefore, if the physical properties of the sample and testing fluid are given and the requirement of small pressure difference is met, the influence of the boundary and initial conditions on the plot of logarithmic differential pressure versus time plot ($\ln \Delta P$ vs. t) can be concluded as:

- (1) The boundary conditions affect slope α and the intercept f .
- (2) The initial condition only affects the intercept f .

3. Implications

3.1. The non-uniform initial pressure distribution

The previous studies (Brace et al., 1968; Tinni et al., 2012) usually require the last pulse to be eliminated and the pressure within the

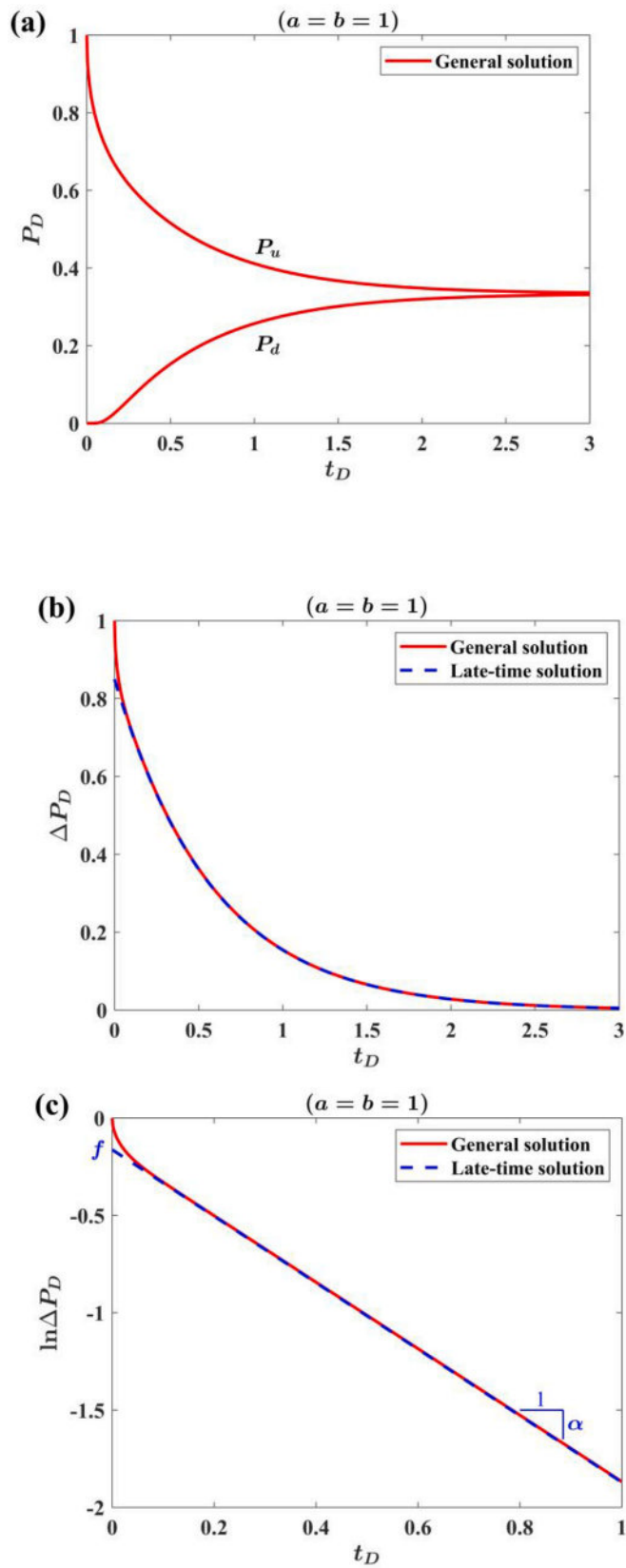


Fig. 3. Comparison of the full general solution (22) and the late-time solution (23) with $\alpha = \beta = 1$. (a) Transients of dimensionless upstream and downstream pressures. (b) Decline of the dimensionless pressure difference (upstream – downstream) with time. (c) Logarithm of the pressure difference as a function of time. The expressions for the slope α and the intercept f are given by Eqs. (25) and (26), respectively.

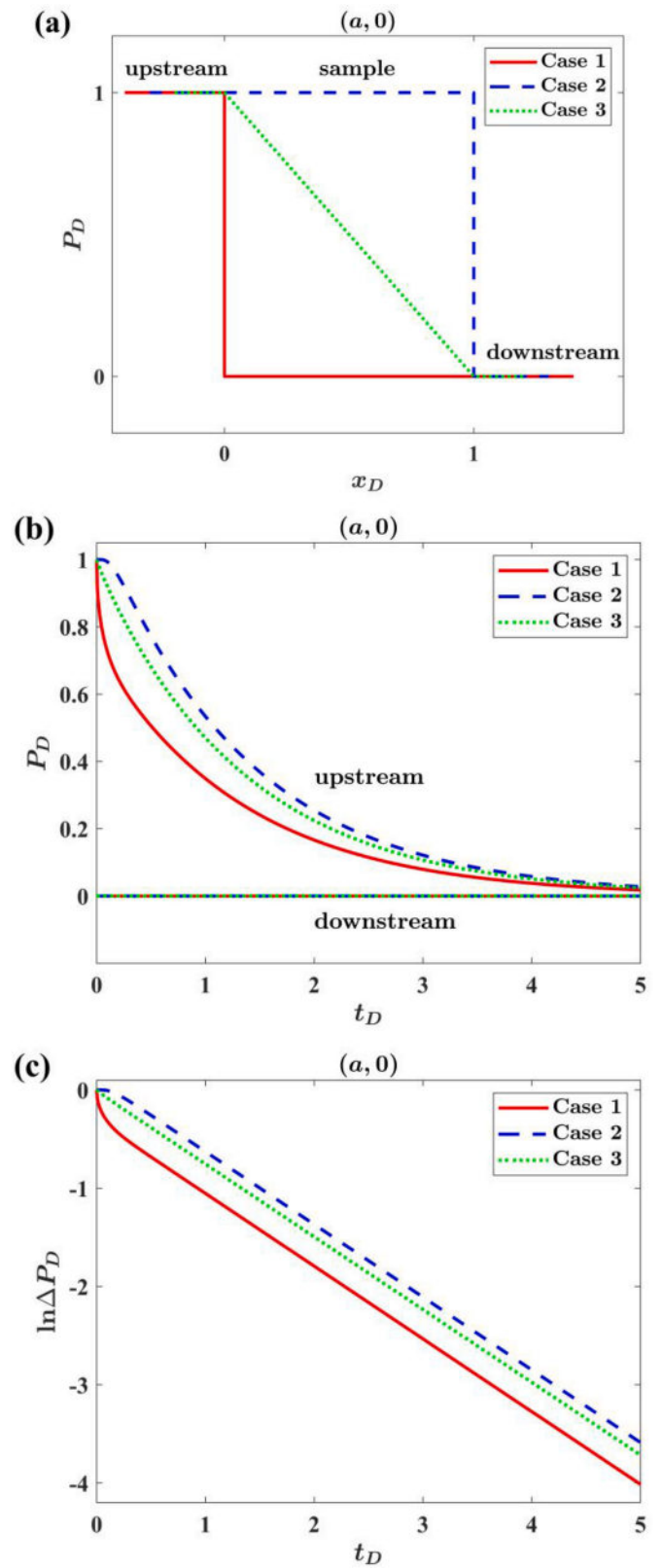


Fig. 4. Numerical simulation of pulse-decay permeability tests with different initial conditions. The downstream pressure is kept constant. (a) The initial conditions corresponding to case 1 to 3. (b) Upstream and downstream pressure transients for the three cases. (c) Logarithm of the differential pressure over time for the three cases.

sample to be uniform before the application of a new pressure pulse (see the two initial conditions in Eq. (7)). Our analysis implies that this is not a necessary requirement for the late-time data processing, because only the slope rather than the intercept is used for permeability evaluation and the former is insensitive to the pressure distribution in the sample when the pressure difference between two ends of the sample is less than 10 %.

To illustrate this point, the pressure variations in pulse-decay methods with the same boundary conditions while with three different initial conditions are solved using MATLAB and the results are shown in Fig. 4. All the variables in the simulation were dimensionless. The governing equation, together with the boundary and initial conditions, are discretized by the finite difference method using the Crank-Nicolson scheme (Crank and Nicolson, 1947). Only the results for the boundary conditions (a, ∞) , where the downstream pressure is kept constant, are shown here, but similar results can be obtained from the other categories of boundary conditions.

Fig. 4(a) gives the initial conditions in the three simulation cases, among which case 3 has a non-uniform pressure distribution and thus moderate initial gas storage within the sample, while case 1 (Empty) and 2 (Loaded) are uniform within the sample and have low and high initial gas storage, respectively. Fig. 4(b) shows the upstream and downstream pressure variations with time. In the three cases, the upstream pressures decrease as time increases until they equal to the downstream pressures, but for any given moment, the case with the higher initial gas storage have the higher upstream pressure (i.e. $P_{ud}^{case2}(t_p) > P_{ud}^{case3}(t_p) > P_{ud}^{case1}(t_p)$). Fig. 4(c) gives the variations of logarithmic differential pressures over time for the three cases. The results show that with different initial conditions, the logarithmic differential pressures in the three cases decay with the same slope but different intercepts shortly after the start of the test.

The numerical simulation results shown in Fig. 4, on the one hand, validate our conclusion in section 2 that when the relative pressure difference is less than 10 %, the intercept f is affected by the initial conditions while the slope α is not. On the other hand, it proves that the requirement that the pressure in the core must be uniform before applying a pressure pulse is unnecessary, because both uniform and non-uniform initial pressure lead to the same slope value, and experimentally only the slope α rather than the intercept f is needed to evaluate the permeability.

3.2. The magnitude of initial pressure difference

Walder and Nur (1986) proved that if the relative pressure difference in the test is less than 10 %, the linear governing equation (4) is valid. Then the permeability of the sample can be evaluated through the slope of the logarithmic differential pressure versus time plot. However, the restriction on the pressure difference has not been strictly observed. Many pulse-decay measurements with pressure differences of more than 10 % have been reported (Metwally and Sondergeld, 2011; Trimmer et al., 1980; Walder and Nur, 1986; Wang et al., 2015), while the determination of permeability coefficients from such experimental data has not been discussed before, to the best of authors' knowledge.

When the initial pressure difference is more than 10 %, the linear governing equation may be invalid, and so is our linear analysis. However, as time increases, the pressure difference continues to decrease. When the pressure difference reduces to 10 %, the linear governing equation becomes valid, and so does our linear analysis. We can take that time as the starting point and analyze whether the subsequent pressure data can be used for permeability evaluation.

Fig. 5 gives a scheme of pulse-decay tests with a relatively large initial pressure difference. Fig. 5(a) shows the upstream and downstream pressure transients $(P_u(t), P_d(t), t \geq 0)$. At the beginning of the test ($t = 0$), the pressure difference between upstream and downstream is more than 10 %, but as time increases, the pressure difference gradually decreases. After a certain moment ($t = \tau$), the pressure difference

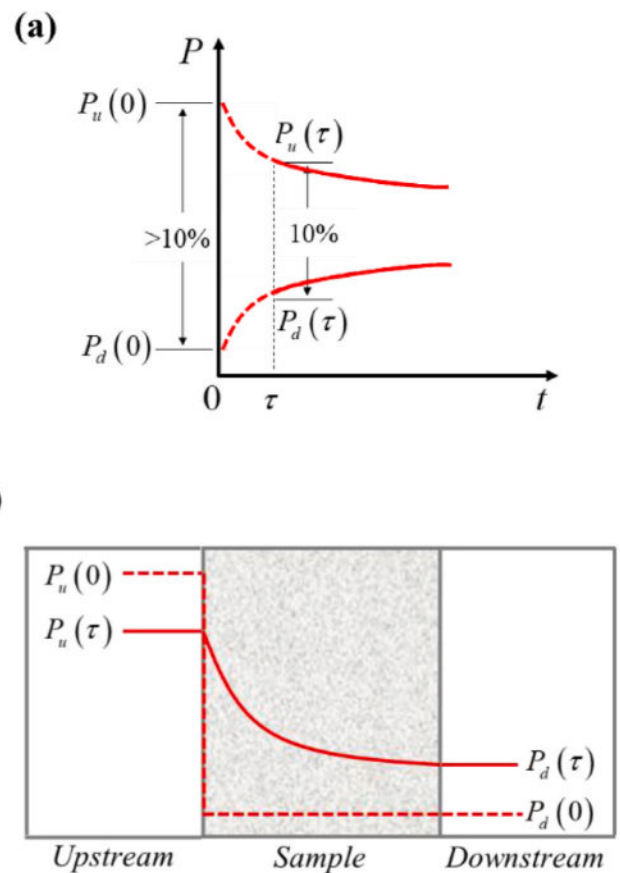


Fig. 5. Scheme of pulse-decay test with a large initial pressure difference. (a) Upstream and downstream pressure transients. Before $t = \tau$, the pressure difference is more than 10 % (dashed line), and after that, the pressure difference becomes smaller than 10 % (solid line). (b) Pressure distribution within the system at $t = 0$ (dashed line) and $t = \tau$ (solid line).

reduces to less than 10 %. Fig. 5(b) gives a scheme of the pressure distribution in the system at $t = \tau$. Since the pulse-decay test has been going on for some time, the pressure distribution within the sample at $t = \tau$ must be non-uniform.

We can regard the pressure transients after time τ ($P_u(t), P_d(t), t \geq \tau$) as the pressure data from a “new” pulse-decay test, which is conducted at time τ and takes the non-uniform pressure distribution in Fig. 5(b) as its initial condition. In the supposed “new” test, the pressure difference is less than 10 %, so the linear governing equation (4) is valid. Based on the linear governing equation and method of separation of variables, we have proved that the non-uniform initial condition has no effects on the linear decline characteristic of logarithmic differential pressure versus time in sections 2 and 3.1. So, if we plot the logarithm of pressure difference after time τ ($\ln \Delta P(t), t \geq \tau$) against time, a straight line can still be obtained, and its slope can be used to evaluate the permeability.

In summary, for the pulse-decay test with a relatively large initial pressure difference, the permeability can still be calculated through the slope of logarithmic differential pressure versus time, as long as we select the data after the pressure difference drops to 10 %. Therefore, the restriction on the pressure difference can be relaxed to some extent. However, technically, an excessive pressure difference should be avoided to protect the core sample from irreversible damage.

4. Experimental validations

Three groups of pulse-decay measurements were conducted to validate the above theoretical analysis. The setup and the experimental protocol have been described in detail in our previous studies (Gaus

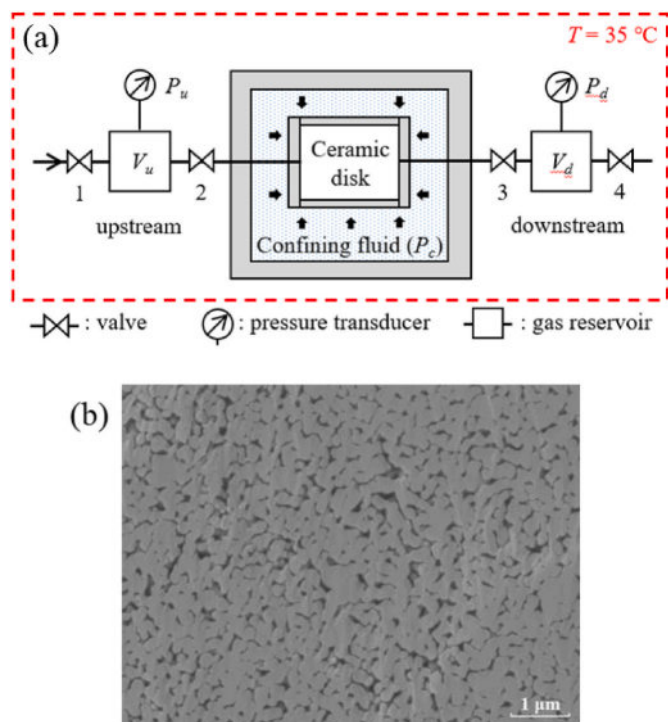


Fig. 6. The setup and the sample used in the pulse-decay measurements. (a) Scheme of the experimental setup. (b) The Broad Ion Beam-Scanning Electron Microscopy (BIB-SEM) image of the ceramic disk. The dark gray and black parts represent the pore space, and the light gray parts represent the Al₂O₃ matrix (Nolte et al., 2021).

Table 2
Parameters of the measurements.

Core sample	Ceramic disk
Testing gas	Helium
Sample length (m)	7.50×10^{-3}
Sample cross section area (m ²)	1.14×10^{-3}
Sample porosity (%)	29
Confining pressure (bar)	200
Equilibrium pore pressure (bar)	1
Temperature (°C)	35

et al., 2019; Nolte et al., 2019; Shabani et al., 2020). The scheme of the setup is shown in Fig. 6(a), and the parameters of the measurements are summarized in Table 2. The sample used in the measurements was a ceramic disk (>99 % Al₂O₃) that is highly homogeneous. The pore structure of the sample was thoroughly characterized by combining low-pressure nitrogen sorption (LPNS) and mercury intrusion porosimetry (MIP). The results are in good agreement and show a narrow and unimodal pore size distribution (with the prominent pore diameter ~70 nm). Fig. 6(b) presents the Broad Ion Beam-Scanning Electron Microscopy (BIB-SEM) image of the ceramic disk. For details of the sample characterization, readers can refer to our previous work (Nolte et al., 2021).

The measurements on the ceramic disk were conducted under the same boundary conditions (a, ∞) (category 2 in Table 1) but with three different initial pressure differences (denoted as test 1 to test 3 in Fig. 7). The parameters of measurements are shown in Table 2. In all tests, the downstream side of the sample was directly open to the atmosphere (constant downstream pressure of 1 atm). The initial pressure differences were realized by increasing the initial upstream pressure to different levels. To ensure the repeatability of the results, four measurements were conducted with the same initial pressure difference. The ceramic disk used here has a very high Young's modulus and is

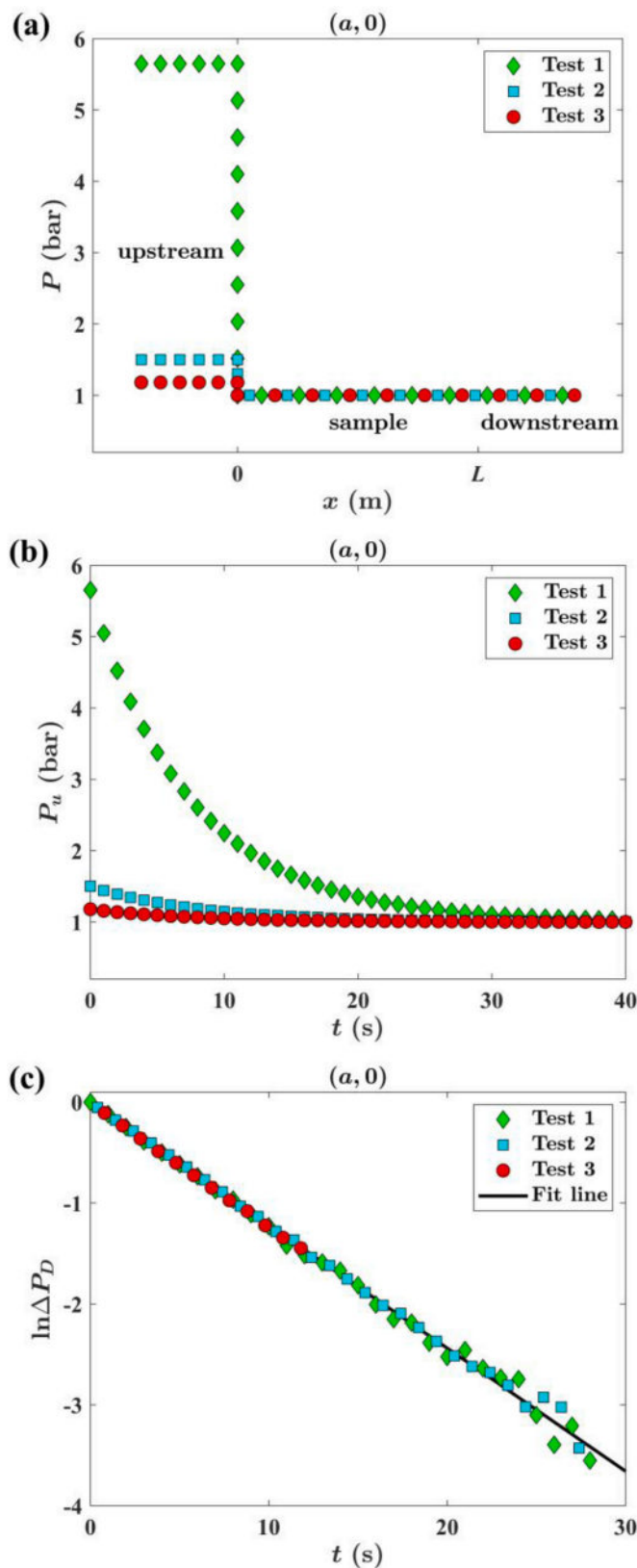


Fig. 7. Pulse-decay tests on a ceramic disk with three different initial pressure differences. (a) The initial pressure distribution of the three tests (b) The changes of upstream pressure over time (c) The selected logarithmic differential pressure data versus time. The solid line denotes the linear fit of the experimental results (scattered points).

insensitive to the effective stress changes during the experiments (Nolte et al., 2021).

Fig. 7(a) gives the initial pressure distribution of the three tests. Except for test 1, the initial pressure differences were more than 10 %. Fig. 7(b) shows the changes of upstream pressure along with time in one series of experiments. As time increased, the upstream pressure in each test finally decreased to the downstream pressure. The logarithms of the differential pressures for selected measurements are plotted versus time in Fig. 7(c), based on which the permeability coefficients can be evaluated ($\sim 900 \mu\text{D}$).

From test 1 to test 3, the number of data points shown in Fig. 7(c) decreases because for the permeability evaluation we only use the data after the relative pressure difference had dropped to 10 %. According to the theoretical analysis in section 3.2, the selected pressure difference data should decline linearly with time in the semi-logarithmic plot, and the slope is proportional to the permeability coefficient. Since the three tests were conducted on one sample with the same final stress condition, their permeability coefficients (and thus slope values) should be the same. In Fig. 7(c), the selected data points of all the three tests showed good linearity and had the same slope, which provides the experimental validation of our theoretical analysis. Because the difference in the intercepts was relatively small, the three sets of data lie essentially on the same line.

5. Discussion

In this section, the influence of the boundary and initial conditions on the time consumption and accuracy of the pulse-decay tests are discussed.

a) Duration of pulse-decay tests

The pulse-decay test starts with applying the pressure pulse and terminate when the pressure difference between the two sides of the sample becomes negligible. To quantitatively investigate the duration of the pulse-decay test, a definite end criterion of the test and an explicit expression for the duration time Γ are both needed. To focus on the influence of the boundary and initial conditions, the physical properties of the rock sample and the testing fluids are all assuming constant.

Here, we define the end of the tests when the dimensionless differential pressure across the sample reduces to 0.05, i.e.

$$\Delta P_D(\Gamma_{0.05}) = \frac{P_u(\Gamma_{0.05}) - P_d(\Gamma_{0.05})}{P_u(0) - P_d(0)} = 0.05 \quad (28)$$

where $\Gamma_{0.05}$ is the dimensionless duration of the pulse-decay test, and the subscript 0.05 denotes the chosen end criterion.

As shown in Fig. 3, the late-time solution (24) approximates the full solution shortly after the start of the test. Substituting Eq. (24) into Eq. (28) and taking the logarithm, we have

$$\ln \Delta P_D(\Gamma_{0.05}) \approx f - \theta_1^2 \Gamma_{0.05} \approx \ln(0.05) \approx -2.996 \quad (29)$$

where f and $-\theta_1^2$ are the intercept and slope of the plot of the logarithm of the differential pressure versus time ($\ln \Delta P_D$ vs. t_D) respectively.

Transforming Eq. (29) yields the expression for $\Gamma_{0.05}$:

$$\Gamma_{0.05} \approx \frac{f + 2.996}{\theta_1^2} \quad (30)$$

Note that θ_1^2 in the denominator of Eq. (30) depends only on the boundary conditions (pore volume/reservoir volume ratios a and b , see Eq. (16)), while f in the numerator rests with both the boundary and initial conditions (see Eq. (25)). The constant 2.996 appearing in the numerator depends on the end criterion of the test, so its value is not unique. For example, the constant will be 4.605 if the pulse-decay test is stopped at a dimensionless differential pressure of 0.01. However, the

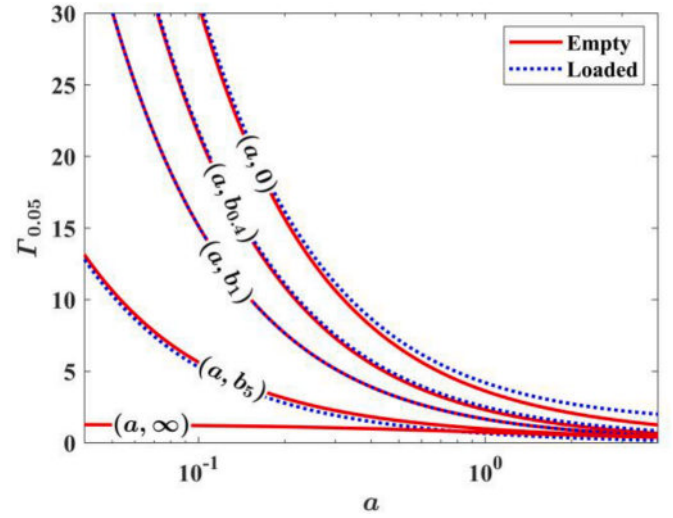


Fig. 8. Duration of the pulse-decay tests with different boundary and initial conditions, where a and b are denoted in Table 1.

value 2.996 here is a good estimate of the order of magnitude.

For pulse-decay tests with different boundary and initial conditions, the durations $\Gamma_{0.05}$ are calculated through Eq. (30), and the results are shown in Fig. 8. Without loss of generality, we only consider the cases where the upstream reservoir has a finite volume, and the downstream reservoir volume can be zero, finite and infinite. The two-element arrays in parentheses in Fig. 8 denote not only the category of boundary condition (see Table 1) but also the relative size of the upstream reservoir to downstream reservoir (e.g. (a, b_5) means $b = 5a$).

Fig. 8 shows that the volume reduction of either the upstream or the downstream (increase of a or b) will shorten the duration of the pulse-decay tests, regardless of the initial condition. Changing the initial condition may increase or decrease the experimental duration, depending on the relative size of the upstream reservoir to the downstream one. Besides, the influence of initial conditions on the duration is only observable when the pore volume/reservoir volume ratios are large but can be ignored when the volume ratios are small (this is usually the case for tight rock measurements).

b) Accuracy of pulse-decay tests

The permeability evaluation in pulse-decay methods needs pore volume/reservoir volume ratios (a and b) as the input (see Eqs. (16) and (27)). Therefore, errors in the pore and reservoir volume measurements will cause errors in the calculation of a and b (abbreviated as volume ratio error). Then the volume ratio error will be transmitted to the permeability evaluation, and such errors are usually non-negligible for tight rocks because their pore volumes are hard to assess accurately. In this section, the error in permeability evaluation in pulse-decay methods due to the volume ratio error is investigated.

The error in permeability measurements is defined as

$$\text{Permeability error} = \frac{k_{\text{error}} - k_{\text{real}}}{k_{\text{real}}} \times 100\% \quad (31)$$

where k_{error} [m^2] is the permeability evaluated through volume ratios with error and k_{real} [m^2] is the permeability evaluated through the real volume ratios. It is noted that the volume ratios only appear in the boundary conditions (see Eq. (6)), rather than the initial conditions. Therefore, the pulse-decay methods with different categories of boundary conditions but the same initial condition are considered here. Without loss of generality, the upstream reservoir in our simulation has a finite volume while the downstream one can be of zero, finite, or infinite volume, and the simulation results are shown in Fig. 9. It is

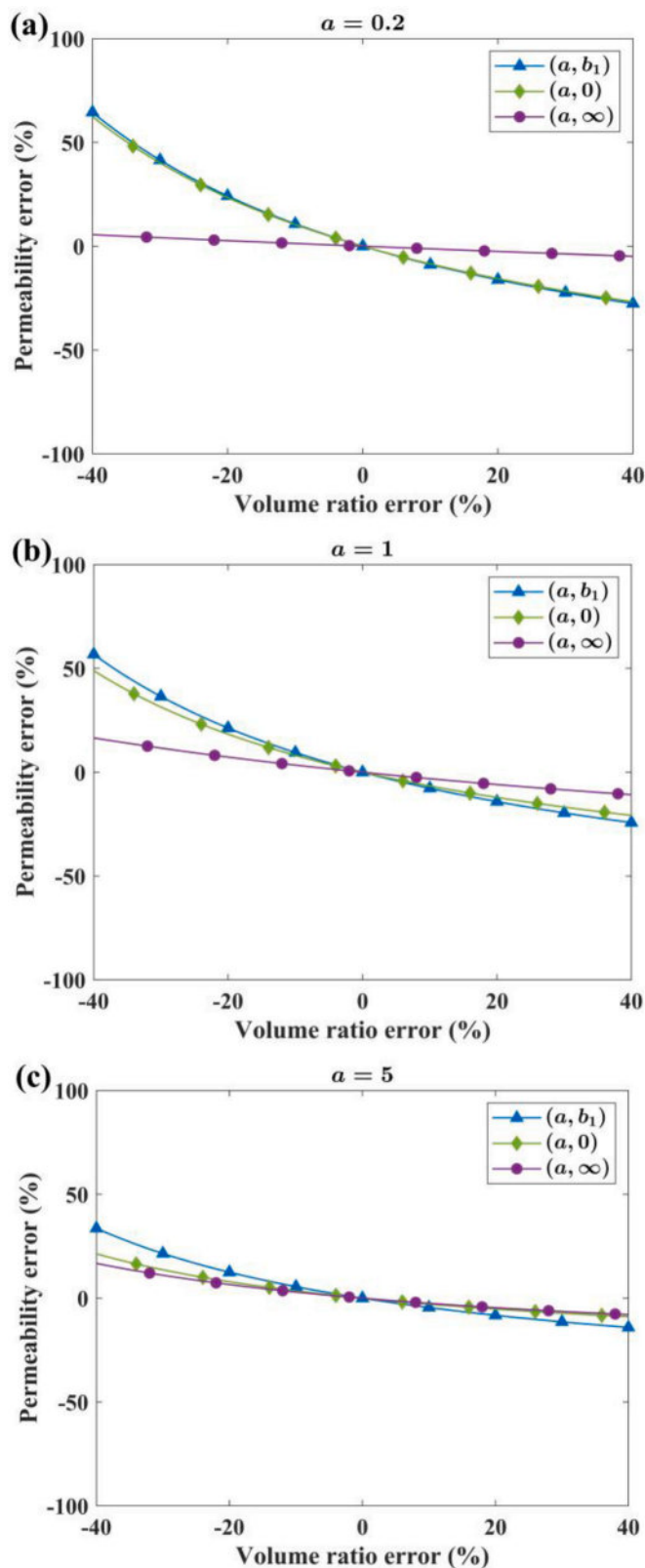


Fig. 9. The permeability error caused by volume ratio error. The results for three boundary conditions and three volume ratios are compared.

found that despite the boundary condition, the permeability error is positive when the volume ratio error is positive, and vice versa. The absolute value of the permeability error increases as that of the volume ratio error increases. Besides, with the same volume ratio error, when

the pore to reservoir volume ratios (a and b) become larger, i.e. smaller gas reservoirs are used, the permeability error will decrease. Therefore, when the upstream reservoirs are kept the same, the boundary condition (a, ∞) , where a reservoir of “zero” volume is used on the downstream side, always has a smaller permeability error compared with the other two boundary conditions, where a downstream reservoir of finite or “infinite” volume is used.

6. Conclusions

In this study, a comprehensive analysis of the pulse-decay methods has been carried out from the perspective of the boundary and initial conditions. Three different typical boundary conditions and two different initial conditions used in previous studies have been analyzed systematically. The testing gas is assumed to be inert to minimize the effect of adsorption. The separation of variables method was applied to obtain the analytical solutions of the pulse-decay process and investigate the influence of the boundary conditions and initial conditions for the first time. The results show that the general solutions of the pulse-decay methods have the forms of infinite series. If the logarithm of the differential pressure is plotted against time, a straight line is obtained at the late-time stage. When the pressure difference between two ends of the sample is less than 10 %, the slope of this line is uniquely determined by the boundary conditions, and the intercept depends on both the boundary and initial conditions.

The results also show that when the restriction on the pressure difference is met, the requirement for the pressure in the sample to be uniform before applying a pressure pulse, which has commonly been adopted in previous studies, is not essential for permeability evaluation. For pulse-decay tests starting with a pressure difference of more than 10 %, the experimental data after the decline of the pressure difference to 10 % can still be used for permeability evaluation, but excessive pressure differences should be avoided to protect the sample from irreversible damages. Numerical simulations and experimental results have been used to verify the above statements.

The duration and accuracy of the pulse-decay methods have also been investigated. We find that for lower pore volume/reservoir volume ratios, i.e. when larger reservoirs are used, the duration of the pulse-decay tests increases. The influence of the initial conditions on the duration is significant when the pore volume/reservoir volume ratios are large, but it decreases as the pore volume/reservoir volume ratios decrease. In pulse-decay methods, the permeability evaluation needs volume ratios as input parameters, so the measurement error of the volume ratios induces a corresponding error in the permeability coefficient. The analysis shows that the smaller the gas reservoirs, the less sensitive the permeability to volume ratio errors. Therefore, using small gas reservoirs can help to shorten the duration and increase the accuracy of the pulse-decay tests.

Credit author statement

Yue Wang: Investigation, Software, Validation, Writing – original draft, Zhiguo Tian: Software, Writing – original draft, Steffen Nolte: Investigation, Experiments, Alexandra Amann: Project administration, Bernhard Krooss: Writing – review & editing, Project administration, Moran Wang: Conceptualization, Supervision, Writing – review & editing, Project administration.

Declaration of competing interest

We declare that there is no Conflict of interests for this work.

Acknowledgements

This work is financially supported by the NSFC Grant (No. U1837602, 11761131012) and the Tsinghua University Initiative

Scientific Research Program. Our simulations are run on the “Explorer 100” cluster of Tsinghua National Laboratory for Information Science

and Technology.

Appendix

Table A-1

Analytical solutions of the pulse-decay method

No.	Boundary conditions	Initial condition	Analytical solution	θ_m
1	(a, b)	Empty	$\Delta P_D^0 = 2 \sum_{m=1}^{\infty} \frac{(a\theta_m^2 + ab^2) + (b\theta_m^2 - ab^2)/\cos \theta_m}{\theta_m^4 + (a^2 + b^2 + a + b)\theta_m^2 + ab(ab + a + b)} e^{-\theta_m^2 t_0}$	$\tan \theta_m = \frac{(a + b)\theta_m}{\theta_m^2 - ab}$
2	(a, b)	Loaded	$\Delta P_D^1 = 2 \sum_{m=1}^{\infty} \frac{(b\theta_m^2 + a^2b) + (a\theta_m^2 - a^2b)/\cos \theta_m}{\theta_m^4 + (a^2 + b^2 + a + b)\theta_m^2 + ab(ab + a + b)} e^{-\theta_m^2 t_0}$	$\tan \theta_m = \frac{(a + b)\theta_m}{\theta_m^2 - ab}$
3	(a, 0)	Empty	$\Delta P_D^2 = 2 \sum_{m=1}^{\infty} \frac{a}{\theta_m^2 + a^2 + a} e^{-\theta_m^2 t_0}$	$\tan \theta_m = \frac{a}{\theta_m}$
4	(a, 0)	loaded	$\Delta P_D^3 = 2 \sum_{m=1}^{\infty} \frac{a}{(\theta_m^2 + a^2 + a)\cos \theta_m} e^{-\theta_m^2 t_0}$	$\tan \theta_m = \frac{a}{\theta_m}$
5	(0, b)	Empty	$\Delta P_D^4 = 2 \sum_{m=1}^{\infty} \frac{b}{(\theta_m^2 + b^2 + b)\cos \theta_m} e^{-\theta_m^2 t_0}$	$\tan \theta_m = \frac{b}{\theta_m}$
6	(0, b)	Loaded	$\Delta P_D^5 = 2 \sum_{m=1}^{\infty} \frac{b}{\theta_m^2 + b^2 + b} e^{-\theta_m^2 t_0}$	$\tan \theta_m = \frac{b}{\theta_m}$
7	(a, ∞)	Empty	$\Delta P_D^{**} = 2 \sum_{m=1}^{\infty} \frac{a}{\theta_m^2 + a^2 + a} e^{-\theta_m^2 t_0}$	$\tan \theta_m = -\frac{\theta_m}{a}$
8	(∞ , b)	Loaded	$\Delta P_D^{***} = 2 \sum_{m=1}^{\infty} \frac{b}{\theta_m^2 + b^2 + b} e^{-\theta_m^2 t_0}$	$\tan \theta_m = -\frac{\theta_m}{b}$

$$\Delta P_D^* = P_{uD}(t_D) - P_{dD}(t_D), \Delta P_D^{**} = P_{uD}(t_D) - P_{uD}(\infty), \Delta P_D^{***} = P_{dD}(\infty) - P_{dD}(t_D)$$

References

Akkutlu, I.Y., Fathi, E., 2012. Multiscale gas transport in shales with local kerogen heterogeneities. *SPE J.* 17, 1,002–1,011, 04.

Bhandari, A.R., Flemings, P.B., Polito, P.J., Cronin, M.B., Bryant, S.L., 2015. Anisotropy and stress dependence of permeability in the Barnett shale. *Transport Porous Media* 108 (2), 393–411.

Billiotte, J., Yang, D., Su, K., 2008. Experimental study on gas permeability of mudstones. *Physics and Chemistry of the Earth. Parts A/B/C* 33, S231–S236.

Birkholzer, J., Houseworth, J., Tsang, C.-F., 2012. Geologic disposal of high-level radioactive waste: status, key issues, and trends. *Annu. Rev. Environ. Resour.* 37, 79–106.

Brace, W.F., Walsh, J., Frangos, W., 1968. Permeability of granite under high pressure. *J. Geophys. Res.* 73 (6), 2225–2236.

Busch, A., Alles, S., Gensterblum, Y., Prinz, D., Dewhurst, D.N., Raven, M.D., Stanjek, H., Krooss, B.M., 2008. Carbon dioxide storage potential of shales. *International journal of greenhouse gas control* 2 (3), 297–308.

Chen, T., Feng, X.-T., Cui, G., Tan, Y., Pan, Z., 2019. Experimental study of permeability change of organic-rich gas shales under high effective stress. *J. Nat. Gas Sci. Eng.* 64, 1–14.

Crank, J., Nicolson, P., 1947. A Practical Method for Numerical Evaluation of Solutions of Partial Differential Equations of the Heat-Conduction Type, *Mathematical Proceedings of the Cambridge Philosophical Society*. Cambridge University Press, pp. 50–67.

Cui, X., Bustin, A., Bustin, R.M., 2009. Measurements of gas permeability and diffusivity of tight reservoir rocks: different approaches and their applications. *Geofluids* 9 (3), 208–223.

Dicker, A., Smits, R., 1988. A practical approach for determining permeability from laboratory pressure-pulse decay measurements. In: *International Meeting on Petroleum Engineering*. Society of Petroleum Engineers.

Dong, J.-J., Hsu, J.-Y., Wu, W.-J., Shimamoto, T., Hung, J.-H., Yeh, E.-C., Wu, Y.-H., Sone, H., 2010. Stress-dependence of the permeability and porosity of sandstone and shale from TCDP Hole-A. *Int. J. Rock Mech. Min. Sci.* 47 (7), 1141–1157.

Fink, R., Krooss, B., Amann-Hildenbrand, A., 2017. Stress-dependence of Porosity and Permeability of the Upper Jurassic Bossier Shale: an Experimental Study. *Special Publications*, vol. 454. Geological Society, London, pp. 107–130, 1.

Gaus, G., Amann-Hildenbrand, A., Krooss, B.M., Fink, R., 2019. Gas permeability tests on core plugs from unconventional reservoir rocks under controlled stress: a comparison of different transient methods. *J. Nat. Gas Sci. Eng.* 65, 224–236.

Hannon, M.J., 2016. Alternative approaches for transient-flow laboratory-scale permeametry. *Transport Porous Media* 114 (3), 719–746.

Heller, R., Vermynen, J., Zoback, M., 2014. Experimental investigation of matrix permeability of gas shales. *Experimental investigation of matrix permeability of gas shales*. AAPG Bull. 98 (5), 975–995.

House, K.Z., Schrag, D.P., Harvey, C.F., Lackner, K.S., 2006. Permanent carbon dioxide storage in deep-sea sediments. *Proc. Natl. Acad. Sci. Unit. States Am.* 103 (33), 12291–12295.

Hsieh, P., Tracy, J., Neuzil, C., Bredehoeft, J., Silliman, S.E., 1981. A Transient Laboratory Method for Determining the Hydraulic Properties of ‘tight’ rocks—I.

Theory, *International Journal of Rock Mechanics and Mining Sciences & Geomechanics Abstracts*. Elsevier, pp. 245–252.

Hu, Z., Klaver, J., Schmatz, J., Dewanckele, J., Littke, R., Krooss, B.M., Amann-Hildenbrand, A., 2020. Stress sensitivity of porosity and permeability of Cobourg limestone. *Eng. Geol.* 273, 105632.

Jones, F.O., Owens, W., 1980. A laboratory study of low-permeability gas sands. *J. Petrol. Technol.* 32, 1,631–1,640, 09.

Jones, S., 1997. A technique for faster pulse-decay permeability measurements in tight rocks. *SPE Form. Eval.* 12, 19–26, 01.

Liu, X., Zhang, D., 2019. A review of phase behavior simulation of hydrocarbons in confined space: implications for shale oil and shale gas. *J. Nat. Gas Sci. Eng.* 68.

Lv, Q., Chen, Z., Wang, M., 2017. An improved elastic-tubes model for the correlation of permeability and stress with correction for the Klinkenberg effect. *J. Nat. Gas Sci. Eng.* 48, 24–35.

Metwally, Y.M., Sondergeld, C.H., 2011. Measuring low permeabilities of gas-sands and shales using a pressure transmission technique. *Int. J. Rock Mech. Min. Sci.* 48 (7), 1135–1144.

Miller, W., Alexander, R., Chapman, N., McKinley, J.C., Smellie, J., 2000. *Geological Disposal of Radioactive Wastes and Natural Analogues*, 2. Elsevier.

Nolte, S., Fink, R., Krooss, B.M., Amann-Hildenbrand, A., Wang, Y., Wang, M., Schmatz, J., Klaver, J., Littke, R., 2021. Experimental investigation of gas dynamic effects using nanoporous synthetic materials as tight rock analogues. *Transport in porous media*.

Nolte, S., Geel, C., Amann-Hildenbrand, A., Krooss, B.M., Littke, R., 2019. Petrophysical and geochemical characterization of potential unconventional gas shale reservoirs in the southern Karoo Basin, South Africa. *Int. J. Coal Geol.* 212, 103249.

Pan, Z., Connell, L.D., 2012. Modelling permeability for coal reservoirs: a review of analytical models and testing data. *Int. J. Coal Geol.* 92, 1–44.

Pan, Z., Connell, L.D., Camilleri, M., 2010. Laboratory characterisation of coal reservoir permeability for primary and enhanced coalbed methane recovery. *Int. J. Coal Geol.* 82 (3–4), 252–261.

Pang, Y., Soliman, M.Y., Deng, H., Emadi, H., 2017. Analysis of effective porosity and effective permeability in shale-gas reservoirs with consideration of gas adsorption and stress effects. *SPE J.* 22, 1739–1759, 06.

Riley, K.F., Hobson, M.P., Bence, S.J., Hobson, M., 2002. *Mathematical methods for physics and engineering: a comprehensive guide*. Cambridge university press.

Sander, R., Pan, Z., Connell, L.D., 2017. Laboratory measurement of low permeability unconventional gas reservoir rocks: a review of experimental methods. *J. Nat. Gas Sci. Eng.* 37, 248–279.

Shabani, M., Krooss, B.M., Hallenberger, M., Amann-Hildenbrand, A., Fink, R., Littke, R., 2020. Petrophysical characterization of low-permeable carbonaceous rocks: comparison of different experimental methods. *Mar. Petrol. Geol.* 122, 104658.

Song, J., Zhang, D., 2013. Comprehensive review of caprock-sealing mechanisms for geologic carbon sequestration. *Environ. Sci. Technol.* 47 (1), 9–22.

Tinni, A., Fathi, E., Agarwal, R., Sondergeld, C.H., Akkutlu, I.Y., Rai, C.S., 2012. Shale Permeability Measurements on Plugs and Crushed Samples, *SPE Canadian Unconventional Resources Conference*. Society of Petroleum Engineers.

Trimmer, D., Bonner, B., Heard, H., Duba, A., 1980. Effect of pressure and stress on water transport in intact and fractured gabbro and granite. *J. Geophys. Res.: Solid Earth* 85 (B12), 7059–7071.

- Walder, J., Nur, A., 1986. Permeability Measurement by the Pulse-Decay Method: Effects of Poroelastic Phenomena and Non-linear Pore Pressure Diffusion, *International Journal of Rock Mechanics and Mining Sciences & Geomechanics Abstracts*. Elsevier, pp. 225–232.
- Wang, L., Chen, Z., Wang, C., Elsworth, D., Liu, W., 2019. Reassessment of coal permeability evolution using steady-state flow methods: the role of flow regime transition. *Int. J. Coal Geol.* 211, 103210.
- Wang, Y., Liu, S., Elsworth, D., 2015. Laboratory investigations of gas flow behaviors in tight anthracite and evaluation of different pulse-decay methods on permeability estimation. *Int. J. Coal Geol.* 149, 118–128.
- Wang, Z., Fink, R., Wang, Y., Amann-Hildenbrand, A., Krooss, B.M., Wang, M., 2018. Gas permeability calculation of tight rocks based on laboratory measurements with non-ideal gas slippage and poroelastic effects considered. *Int. J. Rock Mech. Min. Sci.* 112, 16–24.
- Yang, Y., Wang, M., 2019. Cation diffusion in compacted clay: a pore-scale view. *Environ. Sci. Technol.* 53 (4), 1976–1984.
- Yang, Z., Sang, Q., Dong, M., Zhang, S., Li, Y., Gong, H., 2015. A modified pressure-pulse decay method for determining permeabilities of tight reservoir cores. *J. Nat. Gas Sci. Eng.* 27, 236–246.
- Zoback, M.D., Byerlee, J., 1975. Permeability and effective stress. *AAPG (Am. Assoc. Pet. Geol.) Bull.* 59 (1), 154–158.